Journal of Physics:
Condensed Matter

PAPER

Magnetoelectric and converse magnetoelectric effects in $DyCrO_4$ probed by electron spin resonance

To cite this article: Muhammad Waqas Nafees *et al* 2025 *J. Phys.: Condens. Matter* **37** 385802

IOP Publishing Journal of Physics: Condensed Matter
J. Phys.: Condens. Matter **37** (2025) 385802 (7pp) https://doi.org/10.1088/1361-648X/ae054a

Magnetoelectric and converse magnetoelectric effects in $DyCrO_4$ probed by electron spin resonance

Muhammad Waqas Nafees[1,3,5], Xiao Wang[2,5], Liqin Yan[1,3,*], Fangwei Wang[1,4], Lunhua He[1,4], Jun Lu[1], Tongyun Zhao[1], Fengxia Hu[1], Baogen Shen[1] and Youwen Long[1,*]

[1] Beijing National Laboratory for Condensed Matter Physics, Institute of Physics, Chinese Academy of Sciences, Beijing 100190, People's Republic of China
[2] Institute of Quantum Materials and Physics, Henan Academy of Sciences, Zhengzhou 450046, People's Republic of China
[3] School of Physical Sciences, University of Chinese Academy of Sciences, Beijing 100190, People's Republic of China
[4] Spallation Neutron Source Science Center, Dongguan 523803, People's Republic of China

E-mail: lqyan@iphy.ac.cn and ywlong@iphy.ac.cn

Received 14 July 2025, revised 28 August 2025
Accepted for publication 9 September 2025
Published 18 September 2025

Abstract

This study investigates the magnetoelectric (ME) effect of z-type $DyCrO_4$ and the converse magnetoelectric (CME) effect of s-type $DyCrO_4$ by using electron spin resonance (ESR). The peak-to-peak linewidths (ΔH_{pp}), g-values, and double integral intensities (I) were calculated from the ESR spectra to investigate the coupling behaviors. The ME coupling effect was observed at 135 K in the z-type $DyCrO_4$ powder, evidenced by an anomaly in the temperature dependence of the intensity or g value extracted from ESR. The CME coupling effect was investigated in s-type $DyCrO_4$ pellet, where remarkable intensity changes on the ESR signals, induced by electric field (E), were observed below 24 K. The curves of I versus E at 4 K, 10 K, and 15 K disclosed a temperature-dependent change in magnetization in accordance with the reported CME coupling effect. This study contributes valuable insights into the ME characteristics of $DyCrO_4$ and focuses on the potential of ESR as a powerful tool for investigating these effects in multiferroic materials.

Keywords: electron spin resonance, magnetoelectric effect, converse magnetoelectric effect

1. Introduction

Applications such as sensitive magnetic field sensors, nonvolatile memory, and spintronic devices make use of the linear ME effect and multiferroicity, which enable the control of magnetization (M) and polarization (P) via electric and magnetic fields, respectively [1–6]. The electric polarization and magnetization that result from the linear ME effect are directly proportional to the applied magnetic field and electric field, respectively. This relationship can be expressed quantitatively as $P = \alpha H$ or $\mu_0 M = \alpha E$, where α signifies the linear ME coefficient, while μ_0 represents the magnetic permeability of vacuum [6–8]. The initial discovery of the linear ME effect in chromium oxide (Cr_2O_3) dates back to the 1960 s [9, 10]. Pursuing single-phase ME materials with higher α values has garnered significant interest. Typically, the highest α achieved in nonpolar antiferromagnetic (AFM) structures is less than 40 ps m^{-1}.

[5] Co-first authors.
[*] Authors to whom any correspondence should be addressed.

For practical applications, it is crucial to achieve a larger and more stable ME effect across broader temperature and magnetic field ranges. In the 1990 s, the concept of 'multiferroics' emerged to refer to materials that display multiple ferroic orders—such as ferromagnetism, ferroelectricity, and ferro-elasticity—within a single phase [11]. Particularly, the multiferroics with ferroelectricity induced by specific spin order, commonly referred to as ME multiferroicity, have garnered considerable interest due to their robust ME coupling [12–16]. In the context of magnetic space groups, collinear ferromagnetic (FM) spin arrangements do not disrupt spatial inversion symmetry. As a result, in single-phase ME multiferroics, electric polarization is typically generated by unique AFM or canted AFM spin structures [17]. This leads to a magnetic moment that is insufficiently large for effective manipulation. Achieving a material with a strong coupling between FM and ferroelectric (FE) properties, along with a substantial magnetic moment, presents a significant challenge [18–20].

$DyCrO_4$ is noteworthy due to its unusual Cr^{5+} valence state. At room temperature, it forms a *z*-type crystal structure characterized by the $I4_1/amd$ space group [21, 22]. Additionally, the *z*-type structure exhibits a notable sensitivity to external pressure. Previous studies have documented an irreversible structural phase transition induced by pressure, leading to the formation of a new *s*-type phase characterized by $I4_1/a$ symmetry [23]. Unlike the FM *z*-type phase, the *s*-type phase demonstrates a long-range AFM transition [24–26]. This compound exhibits a nonpolar collinear AFM ground state in the absence of a magnetic field. Within a magnetic field range of $\mu_0 H \approx \pm 3$ T and nearly constant linear ME effect, which allows for magnetic field control of polarization (P) and electric field control of magnetization (M). A metamagnetic transition occurs at high magnetic fields, leading to strong FM magnetization. Furthermore, FE polarization may develop because of the new spin's configuration disruption of spatial inversion symmetry [6]. The ME response in $DyCrO_4$ arises from symmetry-allowed off-diagonal components of the linear ME tensor [6] associated with its magnetic point group 2 m, which permits coupling between orthogonal magnetic and electric field directions [12, 27]. In the *z*-type phase, the direct ME effect is driven by Dy–Cr 4f-3d exchange striction, where magnetic-field-induced spin canting breaks inversion symmetry and induces polarization [28]. In contrast, the *s*-type phase exhibits a converse ME effect below the AFM transition temperature, where an applied electric field perturbs the CrO_4 tetrahedra and Dy–O bonds, thereby modulating Dy–Cr superexchange interactions and inducing magnetization [27]. This dual mechanism establishes $DyCrO_4$ as a rare case where both direct and converse ME couplings co-exist in different structural phases.

In this paper, the *z*-type phase under ambient pressure and moderate temperature and the *s*-type phase under high pressure and moderate temperature of polycrystalline $DyCrO_4$ were successfully synthesized (see the 'Sample synthesis and x-ray diffraction (XRD)' section). We employed the ESR technique to examine the magnetic properties, measuring both *z*-type $DyCrO_4$ powder and *s*-type $DyCrO_4$ pellet within the temperature range of 5–300 K. The ME coupling in *z*-type $DyCrO_4$ and the CME coupling in *s*-type $DyCrO_4$ were thoroughly studied.

2. Experiments

2.1. Sample synthesis and XRD

As detailed in previous research [26], we began by synthesizing a *z*-type precursor at ambient pressure to prepare $DyCrO_4$ samples. The resultant green color *z*-type $DyCrO_4$ powder was then compressed into a cylindrical form measuring 4.0 mm in diameter and 3.0 mm in height. This cylinder was treated in a cubic-anvil high-pressure apparatus, subjected to pressures of 6–8 GPa and temperatures between 700–750 K for 10–30 min, using pyrophyllite as the pressure-transmitting medium. The black color polycrystalline (*s*-type $DyCrO_4$) was obtained when heating ceased, and the pressure was steadily released. XRD with a Rigaku diffractometer, utilizing Cu $K_{\alpha 1}$ radiation at settings of 45 kV and 200 mA was used to confirm the crystal structures of *z*-type and *s*-type $DyCrO_4$, respectively. The schematic structures of the *z*-type and *s*-type of $DyCrO_4$ are shown in figure 1.

2.2. ESR measurements

The ability to probe magnetic interactions with extraordinary sensitivity makes ESR unique among techniques for studying ME or CME coupling effects. Unlike macroscopic measurements, which frequently average out localized effects, ESR gives detailed insights into spin dynamics, local magnetic environments, and anisotropies, tailoring it for detecting subtle interactions that drive ME behavior. Its capability to operate across a wide temperature range and capture dynamic changes in real-time offers significant benefits, mainly in systems with complex coupling mechanisms or low-temperature phase transitions [29, 30]. Furthermore, ESR allows for the finding out of key parameters that describe spin interactions and relaxation mechanisms, including ΔH_{pp}, I, and the g-factor. The ΔH_{pp} observed in the ESR signal is closely linked with the interactions between the spins and their local environment [31–33]. Thermal activation models are frequently used to represent the double integral intensity, $I(T)$, which reflects the spin density, especially in the FM phase [34]. The g-factor, taken from the resonance line, signifies the strength of the spin–orbit coupling at the microscopic level. As the temperature nears the critical value (T_c) from above, the ΔH_{pp} typically shows a linear reduction, which is attributed to relaxation processes that are narrowed due to the movement of spins in systems containing FM clusters [29, 30, 34–39].

The ESR experiments were conducted using a JEOL JES-FA200 ESR spectrometer, operating at X-band frequencies of approximately 9.1 GHz, across a temperature range of 4–300 K. The microwave power was maintained at 1 mW. For the ESR measurements of *s*-type $DyCrO_4$, a pellet with a thickness of 0.25 mm was used; The external magnetic field H was applied perpendicular to the pellet plane, and the electric

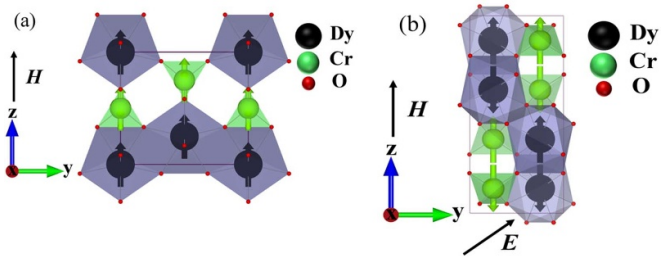

Figure 1. The schematic structures of (a) z-$DyCrO_4$ and (b) s-$DyCrO_4$. Directions of spin moments are indicated by arrows. The external magnetic field H and electric field E were applied perpendicular and parallel to the pellet plane, respectively.

field E was applied parallel to the pellet plane, as shown in figure 1.

3. Results and discussion

Figure 2 displays the selected ESR spectra for powder z-type $DyCrO_4$ across a temperature range from 5 to 300 K. At low temperatures (5–70 K), no distinct resonance peak is observed. However, between 5 and 24 K, the resonance line exhibits a broad asymmetric shape (5–24 K). This atypical line shape points to significant magnetic interactions or local crystal field inhomogeneities. Notably, these features become prominent just below the reported Curie temperature ($T_c \approx 23$ K), suggesting that the observed ESR behavior is closely related to the onset of FM ordering [26]. Between 90 K and 125 K, the spectra indicate the coexistence of paramagnetic (PM) (g) and FM (left dashed line) resonance signals. The intensities of both PM (g) and FM (left dashed line) signals increase with increasing T, observed by distinct trends at specific magnetic fields: near $H = 300$ mT. The intensity of the distorted PM resonance signal increases with increasing T, while the sharp FM peak around $H = 100$ mT is intensified from 100 to 135 K. These observations suggest the presence of magnetic correlations among FM clusters within a PM matrix [38, 40, 41]. Such correlations likely stem from various exchange interactions among the correlated magnetic spins, such as Dy^{3+}-$O^{2-}Dy^{3+}$ or Dy^{3+}-$O^{2-}Cr^{5+}$-$O^{2-}Dy^{3+}$. At 135 K, which is the FE to paraelectric transition temperature T_E reported by [42], the peaks of FM and PM start to distort more, as indicated by the symbol '♥'in figure 2. Above T_E, the distorted FM peaks shift continuously to higher H, as shown in the left dashed line in figure 2, while PM resonance signals become broadened. This reflects the suppression in spin alignment and dissolved magnetic clusters. All resonance lines show significant broadening and splitting characteristics that persist up to 300 K.

The g-factor derived from the resonance line indicates the features of microscopic spin–orbit coupling. It can be expressed as follows [43]:

$$g_J = 1 + \frac{J(J+1) + S(S+1) - L(L+1)}{2J(J+1)}. \qquad (1)$$

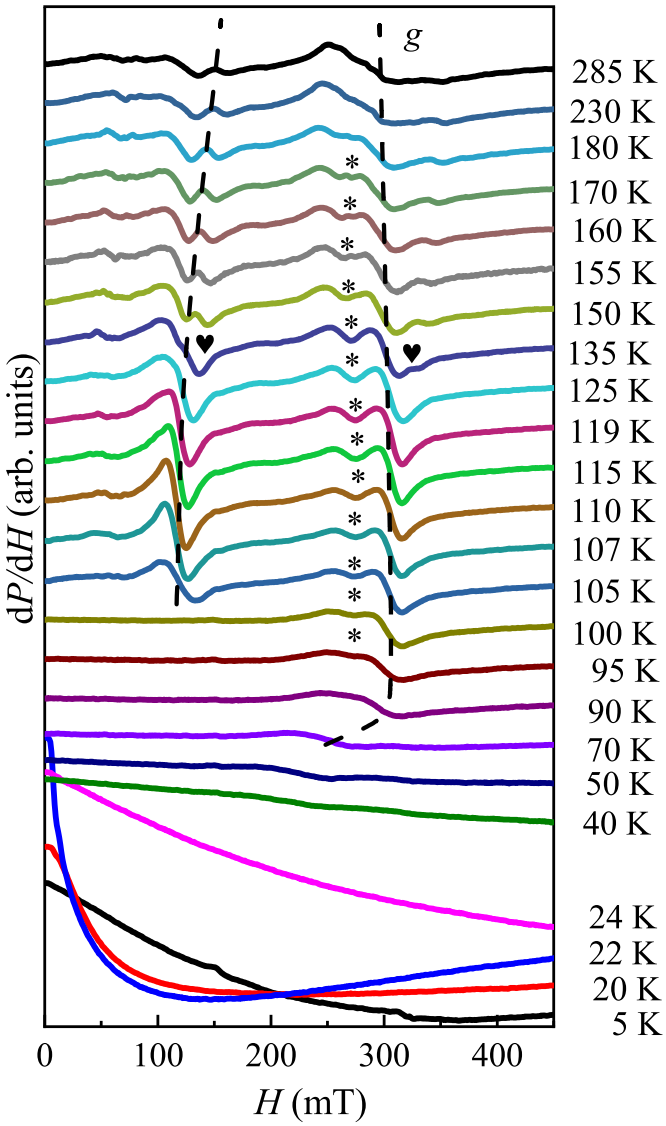

Figure 2. ESR spectra of z-type $DyCrO_4$ powder in the temperature range of 5–285 K. The peaks chosen for extracting the g-factor are indicated by a right curved dashed line. The black symbols '*' and '♥' specify the splitting of peaks.

Here, S, L, and J represent the spin, orbital, and total angular momentum, respectively.

The temperature-dependent g (figure 3) extracted from ESR spectra reveals the anisotropic nature of Dy^{3+} and Cr^{5+} ions in the z-type $DyCrO_4$ lattice. Below T_E, g exhibits a significant decrease, indicating the emergence of magnetic correlations and spin anisotropy due to Dy^{3+} and Cr^{5+} spin interactions [26]. At higher temperatures, the g-value is stabilized, corresponding to the PM regime. The change of g value at T_E implies the occurrence of CME.

The intensity, $I(T)$ (extracted from the double integration of the first derivative spectra, dP/dH), as shown in figure 3, is proportional to the number of spins and is typically explained by using a thermal activation model [34]. A notable rise in $I(T)$ indicates a significant enhancement in spin alignment with

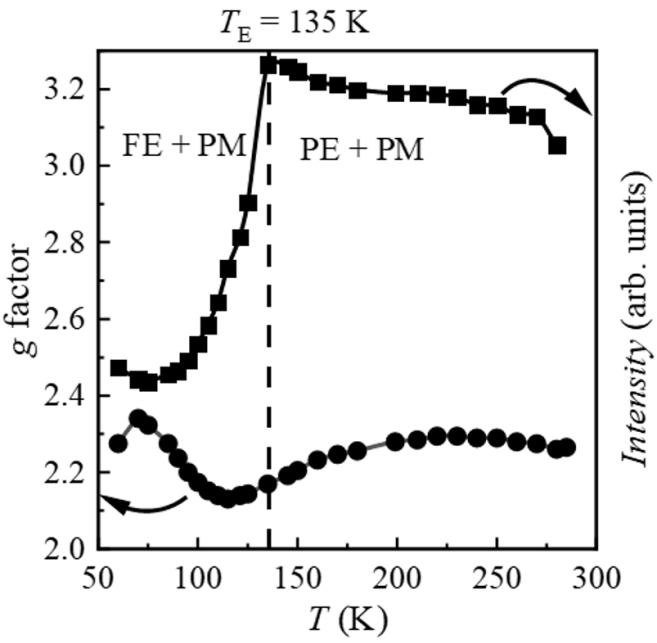

Figure 3. The temperature dependences of the *g* factor and double integral intensity (*I*) of *z*-$DyCrO_4$ powder with a dashed line at T_E (135 K) indicating FE ordering temperature.

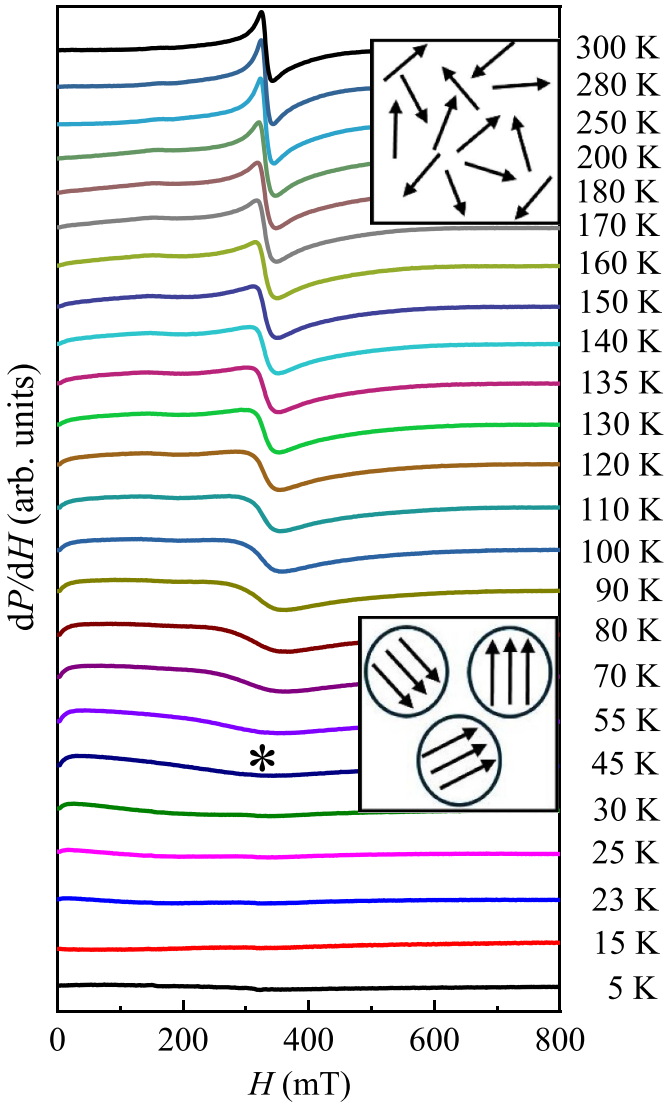

Figure 4. ESR spectra of *s*-type $DyCrO_4$ pellet in the temperature range of 5–300 K. The black symbol '*' indicates the broadening of the spectra at 45 K. The Insets show the spin cluster state and isolated spin PM state, respectively.

increasing *T*, reaching a maximum value at T_E [42], further implying the existence of CME in *z*-type $DyCrO_4$ [26, 44].

Figure 4 presents the selected ESR spectra of *s*-type $DyCrO_4$ pellet measured from 5 to 300 K under a magnetic field of 0–1 T. Below the reported Néel temperature ($T_N \approx 21$ K), no resonance signals are detected, suggesting that the observed ESR behavior is closely related to the onset of AFM ordering [26]. Above T_N, a broadened spectrum appears around $H = 320$ mT, as indicated by the symbol black '*' in figure 4, suggesting PM correlation has emerged. At temperatures above 80 K, the broadening becomes more pronounced, reflecting enhanced spin fluctuations and possibly short-range magnetic correlations that are typical in the PM state. This suggests the evolution from a cluster state to an isolated PM state, as shown in the schematic insets of figure 3. Above 80 K, with further increasing *T*, the resonance peak shape becomes narrower gradually to room temperature. In the temperature range of 135–300 K, the spectra display single Lorentzian curves with narrow widths, indicative of a PM phase where thermal energy dominates, resulting in disordered spins and negligible spin–spin or exchange interactions [41, 43, 44].

The peak-to-peak linewidth ΔH_{pp} of the ESR signal, as shown in figure 5, is intricately linked to the spin interactions with their surroundings [31–33]. With increasing *T*, ΔH_{pp} decreases monotonously, indicating that the magnetic interactions are weakened. An abrupt reduction of ΔH_{pp} is observed from 80 K to 135 K, driven by thermal energy induced a pronounced reduction of exchange interactions. Above 135 K, ΔH_{pp} value decreases linearly, indicating the transition into a fully PM phase, where the thermal energy dominates over the spin ordering [45]. This transition at 135 K, similar to the magnetic transition behaviors of $RCrO_4$ (where R represents elements like Dy, Sm, Eu, and Lu), arises from the exchange interactions between Cr^{5+} ions facilitated by Cr^{5+}-O-O-Cr^{5+} superexchange coupling [46–50]. The linear decrease of ΔH_{pp} above 135 K should be attributed to the increasing electron-phonon interactions [45]. The temperature dependence of *I* derived from figure 4 is also shown in figure 5. It is increasing with rising temperature up to 135 K; this increase should be closely correlated with the Cr^{5+}-O-O-Cr^{5+} superexchange coupling [46–50], which is not detected by the magnetization measurements.

Above 135 K, *I* begins to decrease, confirming the transition from PM cluster to isolated spin state due to thermal fluctuations, as shown in the schematic insets of figure 5. This behavior is consistent with the susceptibility and specific heat measurements reported for *s*-type $DyCrO_4$ [26].

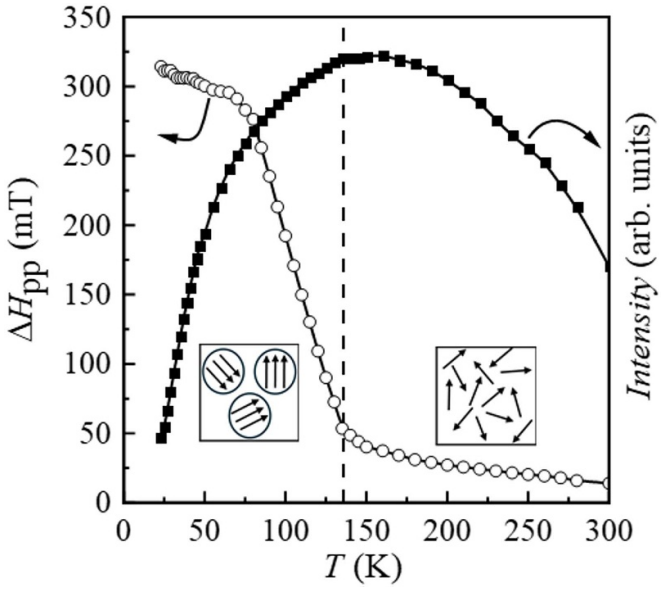

Figure 5. Peak-to-peak linewidth (ΔH_{pp}) and double integral intensity (I) trend of s-type $DyCrO_4$ pellet at the temperature range 23–300 K as a function of temperature. The Insets show the spin cluster state and isolated spin PM state, respectively.

Shen *et al* have studied the linear CME coupling effect below 24 K in s-type $DyCrO_4$ [6]. The CME driven by H induced strong coupled canted ferromagnetism–ferroelectricity, is displayed with a noteworthy magnetic moment change by E [6]. In the current study, the CME coupling effect of s-type $DyCrO_4$ is observed by applying electric potential, E_P (0–480 kV m^{-1}) in combination with varying H (0–1 T) at temperatures of 4 K, 10 K, and 15 K, respectively. The copper wire is affixed to the s-type $DyCrO_4$ pellet (thickness: 0.25 mm) using silver paste. To minimize the generation of eddy current during measurements, the copper wire was subsequently twisted. The pellet is then positioned in the sample holder of an ESR apparatus. A Keithley 6517B electrometer was employed for precise voltage control. The goal of this experimental setup and methodology is to comprehensively investigate how the electric field and magnetic field interact in the material that exhibits complex multiferroic properties. The selection of temperature ranges (4 K, 10 K, and 15 K) is crucial, as it enables the study of the material's reaction across different phases, containing its AFM and field-induced weak FM states [6]. Moreover, the use of ESR gives valuable information on the magnetic ordering and spin dynamics of the material, which is directly affected by the applied E_P, thus validating the existence of the CME effect in s-type $DyCrO_4$. The ESR signals shown in figure 6(a) explain how the material's magnetic spins react to applied H under varying E at 4 K. The ESR signals were noted for applied voltages ranging from 0 to 120 V and then reversed. The observed trend specifies a decrease in intensity with increasing voltage, which shows the existence of CME of s-type $DyCrO_4$. i.e. the change of magnetization induced by the electric field. The intensity (I) values calculated at 4 K, 10 K, and 15 K are shown in figure 6(b). One can see

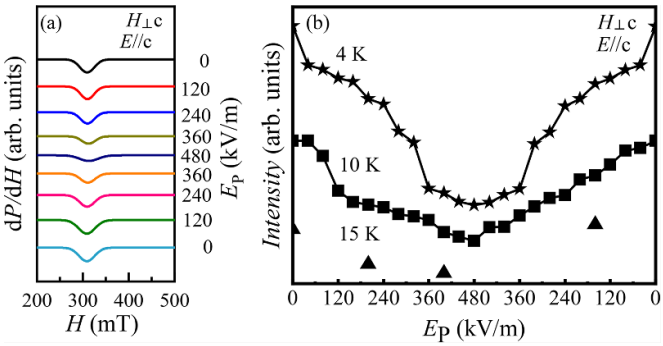

Figure 6. ESR spectra at 4 K (a) and the double integral intensity (I) at 4 K, 10 K, and 15 K (b) of the s-type $DyCrO_4$ pellet as a function of H and E, where $H \perp c$ and $E//c$.

that the electric field depressed the intensity, which is consistent with the reported magnetization measurements under $E_P = \pm 1.08\,MV\ m^{-1}$ [6]. The CME at $E_P = 480$ kV m^{-1} is suppressed as the values of 69.50%, 70.11% and 80.51% at 4 K, 10 K, and 15 K, respectively. It disappeared above T_N. This alignment validates that the CME effect, as investigated by ESR, is providing insights into the material's behavior at the microscopic level. The observed decrease of I with E and the T indicates a strong coupling between the electric field and magnetism below T_N. This behavior highlights the potential of s-type $DyCrO_4$ as a multiferroic material with noteworthy CME coupling, providing an opportunity for further exploration of its applications in spintronic devices and field-tunable magnetic systems.

4. Conclusions

In this study, we successfully synthesized both zircon-type and scheelite-type $DyCrO_4$, yielding homogeneous and single-phase materials. The structural properties of the synthesized compounds were confirmed using x-ray diffraction analysis [44]. The ME and CME coupling effects were effectively investigated by using the ESR technique. The ME coupling effect was clearly observed at 135 K in the z-type $DyCrO_4$ powder, whereas the CME coupling effect was demonstrated in s-type $DyCrO_4$ below 24 K, with significant E changes of ESR $I(M)$ at 4 K, 10 K, and 15 K. These results not only enhance our understanding of the ME characteristics of $DyCrO_4$ but also establish ESR as an effective method for investigating such effects at the microscopic level. These results contribute to the growing field of multiferroic materials, primarily for use in the ME devices and tunable magnetic systems.

Data availability statement

The data cannot be made publicly available upon publication because they contain commercially sensitive information. The data that support the findings of this study are available upon reasonable request from the authors.

Acknowledgment

This work was supported by the National Key R&D Program of China (Grant No. 2021YFA1400300), the National Natural Science Foundation of China (Grant Nos. 52088101, 12174425, 12425403, 12261131499, and U23A20550).

ORCID iDs

Muhammad Waqas Nafees 0009-0005-9041-9917
Xiao Wang 0000-0001-8139-4192
Liqin Yan 0000-0002-2771-7752
Jun Lu 0000-0003-3009-6683
Youwen Long 0000-0002-8587-7818

References

[1] Dong S, Liu J-M, Cheong S-W and Ren Z 2015 Multiferroic materials and magnetoelectric physics symmetry, entanglement, excitation, and topology *Adv. Phys.* **64** 519–626
[2] Fusil S, Garcia V, Barthélémy A and Bibes M 2014 Magnetoelectric devices for spintronics *Annu. Rev. Mater. Res.* **44** 91–116
[3] Ma J, Hu J, Li Z and Nan C-W 2011 Recent progress in multiferroic magnetoelectric composites: from bulk to thin films *Adv. Mater.* **23** 1062–87
[4] Ortega N, Kumar A, Scott F and Katiyar R S 2015 Multifunctional magnetoelectric materials for device applications *J. Phys.: Condens. Matter* **27** 504002
[5] Ramesh R and Spaldin N A 2007 Multiferroics: progress and prospects in thin films *Nat. Mater.* **6** 21–29
[6] Shen X *et al* 2019 Large linear magnetoelectric effect and field-induced ferromagnetism and ferroelectricity in $DyCrO_4$ *npg Asia Mater.* **11** 50
[7] Rivera J-P 2009 A short review of the magnetoelectric effect and related experimental techniques on single phase (multi-) ferroics *Eur. Phys. J. B* **71** 299–313
[8] Fiebig M 2005 Revival of the magnetoelectric effect *J. Phys. D* **38** R123
[9] Astrov D 1960 The magnetoelectric effect in antiferromagnetics *Sov. Phys. JETP* **11** 708–9
[10] Dzyaloshinskii I E 1960 On the magneto-electrical effects in antiferromagnets *Sov. Phys. JETP* **10** 628–9
[11] Schmid H 1994 Multi-ferroic magnetoelectrics *Ferroelectrics* **162** 317–38
[12] Eerenstein W, Mathur N and Scott J F 2006 Multiferroic and magnetoelectric materials *Nature* **442** 759–65
[13] Zhou L *et al* 2017 Realization of large electric polarization and strong magnetoelectric coupling in $BiMn_3Cr_4O_{12}$ *Adv. Mater.* **29** 1703435
[14] Zhang S, Yu R, Azuma M, Shimakawa Y, Zhang H, Dong S, Sun Y, Jin C and Long Y 2015 Observation of magnetoelectric multiferroicity in a cubic perovskite system: $laMn_3Cr_4O_{12}$ *Phys. Rev. Lett.* **115** 087601
[15] Tokura Y, Seki S and Nagaosa N 2014 Multiferroics of spin origin *Rep. Prog. Phys.* **77** 076501
[16] Kimura T, Goto T, Shintani H, Ishizaka K, Arima T and Tokura Y 2003 Magnetic control of ferroelectric polarization *Nature* **426** 55–58
[17] Tokura Y and Seki S 2010 Multiferroics with spiral spin orders *Adv. Mater.* **22** 1554–65
[18] Zhao Z Y, Zhao X, Zhou H D, Zhang F B, Li Q J, Fan C, Sun X F and Li X G 2014 Ground state and magnetic phase transitions of orthoferrite $DyFeO_3$ *Phys. Rev. B* **89** 224405
[19] Kim J-Y, Koo T and Park J-H 2006 Orbital and bonding anisotropy in a half-filled $GaFeO_3$ magnetoelectric ferrimagnet *Phys. Rev. Lett.* **96** 047205
[20] Oh Y S, Artyukhin S, Yang J J, Zapf V, Kim J W, Vanderbilt D and Cheong S-W 2014 Non-hysteretic colossal magnetoelectricity in a collinear antiferromagnet *Nat. Commun.* **5** 3201
[21] Steiner M, Dachs H and Ott H 1979 The determination of the magnetic structure of $DyCrO_4$ by neutron diffraction *Solid State Commun.* **29** 231–4
[22] Tezuka K and Hinatsu Y 2001 Magnetic and crystallographic properties of $LnCrO_4$ (Ln= Nd, Sm, and Dy) *J. Solid State Chem.* **160** 362–7
[23] Long Y W, Yang L X, Yu Y, Li F Y, Lu Y X, Yu R C, Liu Y L and Jin C Q 2008 High-pressure Raman scattering study on zircon-to scheelite-type structural phase transitions of $RCrO_4$ *J. Appl. Phys.* **103** 093542
[24] Santos-García A J D, Climent-Pascual E, Rabie M G, Paz J R D, Amores J M G, Khalyavin D and Sáez-Puche R 2014 Determination of the crystal and magnetic structure of the $DyCrO_4$-scheelite polymorph by neutron diffraction *J. Phys.* **549** 012021
[25] Ray A and Maitra T 2015 Nature of transport gap and magnetic order in zircon and scheelite type $DyCrO_4$ from first principles *J. Phys.: Condens. Matter* **27** 105501
[26] Long Y, Liu Q, Lv Y, Yu R and Jin C 2011 Various 3d-4f spin interactions and field-induced metamagnetism in the Cr^{5+} system $DyCrO_4$ *Phys. Rev. B* **83** 024416
[27] Fiebig M, Lottermoser T, Meier D and Trassin M 2016 The Evolution of multiferroics *Nat. Rev. Mater.* **1** 16046
[28] Cheong S-W and Mostovoy M 2007 Multiferroics: a magnetic twist for ferroelectricity *Nat. Mater.* **6** 1
[29] Houze E and Nechtschein M 1996 ESR in conducting polymers: oxygen-induced contribution to the linewidth *Phys. Rev. B* **53** 14309
[30] Huber D 1998 Analysis of electron paramagnetic resonance experiments in colossal magnetoresistance materials *J. Appl. Phys.* **83** 6949–51
[31] Huber D 2014 Exchange narrowing of the phonon contribution to the electron spin resonance line width in exchange-coupled magnetic insulators *J. Phys.: Condens. Matter* **26** 056002
[32] Seidov Z, Açıkgöz M, Kazan S and Mikailzade F 2016 Magnetic properties of Co_3O_4 polycrystal powder *Ceram. Int.* **42** 12928–31
[33] Acikgoz M and Huber D L 2018 Exchange narrowing of the one-and two-phonon contributions to the electron spin resonance linewidth in Co_3O_4 *J. Magn. Magn. Mater.* **458** 232–4
[34] Joshi J P, Gupta R, Sood A K, Bhat S V, Raju A R and Rao C N R 2001 Temperature-dependent electron paramagnetic resonance studies of charge-ordered $Nd_{0.5}Ca_{0.5}MnO_3$ *Phys. Rev. B* **65** 024410
[35] Matthews M J, Dresselhaus M S, Kobayashi N, Enoki T, Endo M and Nishimura K 1999 Localized spins in partially carbonized polyparaphenylene *Phys. Rev. B* **60** 4749
[36] Houzé E, Nechtschein M and Pron A 1997 Fixed-spin-induced ESR linewidth and polaron mobility in conducting polymers *Phys. Rev. B* **56** 12263
[37] Rettori C, Rao D, Singley J, Kidwell D, Oseroff S B, Causa M T, Neumeier J J, McClellan K J, Cheong S-W and Schultz S 1997 Temperature dependence of the ESR linewidth in the paramagnetic phase ($T > T_C$) of $R_{1-x}B_xMnO_{3+\delta}$ (R= La,Pr;B= Ca,Sr) *Phys. Rev. B* **55** 3083
[38] Yuan S L *et al* 2000 Origins of both insulator–metal transition and colossal magnetoresistance in doped manganese perovskites *Appl. Phys. Lett.* **77** 4398–400

[39] Tovar M *et al* 1998 Electron spin resonance and magnetization in perovskite and pyrochlore manganites *J. Appl. Phys.* **83** 7201–3
[40] Rivadulla F, Freita-Alvite M, López-Quintela M A, Hueso L E, Miguéns D R, Sande P and Rivas J 2002 Coexistence of paramagnetic-charge-ordered and ferromagnetic- metallic phases in $La_{0.5}Ca_{0.5}MnO_3$ evidenced by electron spin resonance *J. Appl. Phys.* **91** 785–8
[41] Yang Z, Bao X, Tan S and Zhang Y 2004 Magnetic polaron conduction in the colossal magnetoresistance material $Fe_{1-x}Cd_xCr_2S_4$ *Phys. Rev. B* **69** 144407
[42] Indra A and Giri S 2019 Multiferroic order and re-entrant spin-glass-like state in $DyCrO_4$ *J. Magn. Magn. Mater.* **489** 165467
[43] Nave C R 2012 *Hyperphysics* (Georgia State University Canada)
[44] He J-C *et al* 2023 Magnetic-field-induced sign changes of thermal expansion in $DyCrO_4$ *Chin. Phys. Lett.* **40** 066501
[45] Yuan S L, Li G, Jiang Y, Li J Q, Zeng X Y, Yang Y P, Huang Z and Jin S Z 2000 Exchange-narrowing spin-spin interaction in the paramagnetic regime of perovskite manganites studied through the EPR measurements for $(La,Y)_{2/3}(Ca, Sr, Ba)_{1/3}MnO_3$ with a wide span of Tc *J. Phys. Condens. Matt.* **12** L109
[46] Jiménez E, Isasi J, Fernández M T and Sáez-Puche R 2002 Magnetic behavior of $ErCrO_4$ oxide *J. Alloys Comp.* **344** 369–74
[47] Puche R S, Climent E, Rabie M G, Romero J and Gallardo J M 2011 Neutron diffraction characterization and magnetic properties of the scheelite-type $ErCrO_4$ polymorph *J. Phys.* **325** 012012
[48] Walter H, Kahle H H, Mulder K and Schoopper H C 1973 Magnetic phase transitions in rare earth chromate *Int. J. Magn.* **5** 129–35
[49] Jiménez E, Isasi J and Sáez-Puche R 2000 Synthesis, structural characterization and magnetic properties of $RCrO_4$ oxides, R= Nd, Sm, Eu and Lu *J. Alloys Compd.* **312** 53–59
[50] Borang O, Srinath S, Kaul S N and Sundarayya Y 2022 Temperature assisted size dependent synthesis and magnetic properties of rare-earth chromium oxide nanoparticles *J. Magn. Magn. Mater.* **562** 169807